catalysts

MDPI

Article

Multitarget Evaluation of the Photocatalytic Activity of P25-SiO_2 Prepared by Atomic Layer Deposition

Miguel Martín-Sómer [1], Dominik Benz [2], J. Ruud van Ommen [2,*] and Javier Marugán [1,*]

[1] Department of Chemical and Environmental Technology, Universidad Rey Juan Carlos, C/Tulipán s/n, 28933 Móstoles, Madrid, Spain; miguel.somer@urjc.es

[2] Department of Chemical Engineering, Delft University of Technology, Mekelweg 5, 2628 CD Delft, The Netherlands; D.Benz@tudelft.nl

* Correspondence: j.r.vanOmmen@tudelft.nl (J.R.v.O.); javier.marugan@urjc.es (J.M.); Tel.: +34-491-664-7466 (J.M.)

Received: 25 February 2020; Accepted: 21 April 2020; Published: 22 April 2020

Abstract: This work presents the evaluation of the photocatalytic activity of P25 TiO_2 particles, coated with SiO_2, using atomic layer deposition (ALD) for the photocatalytic removal of methylene blue, oxidation of methanol and inactivation of *Escherichia coli* bacteria in water and its comparative evaluation with bare P25 TiO_2. Two different reactor configurations were used, a slurry reactor with the catalyst in suspension, and a structured reactor with the catalyst immobilized in macroporous foams, that enables the long-term operation of the process in continuous mode, without the necessity of separation of the particles. The results show that the incorporation of SiO_2 decreases the efficiency of the photocatalytic oxidation of methanol, whereas a significant improvement in the removal of methylene blue is achieved, and no significant changes are observed in the photocatalytic inactivation of bacteria. Adsorption tests showed that the improvements, observed in the removal of methylene blue by the incorporation of SiO_2, was mainly due to an increase in its adsorption. The improvement in the adsorption step as part of the global photocatalytic process led to a significant increase in its removal efficiency. Similar conclusions were reached for bacterial inactivation where the loss of photocatalytic efficiency, suggested by the methanol oxidation tests, was counteracted with a better adherence of bacteria to the catalyst that improved its elimination. With respect to the use of macroporous foams as support, a reduction in the photocatalytic efficiency is observed, as expected from the decrease in the available surface area. Nevertheless, this lower efficiency can be counteracted by the operational improvement derived from the easy catalyst reuse.

Keywords: atomic layer deposition; water treatment; photocatalysis; TiO_2-SiO_2; immobilized photocatalyst; methylene blue adsorption

1. Introduction

Among the photochemical processes, heterogeneous photocatalysis stands out as one of the most attractive processes for the treatment of effluents with contaminants that cannot be eliminated by conventional water treatment technologies. Photocatalysis has the advantage of having simple operating conditions since it can be carried out at ambient temperature and pressure, using the oxygen from the air as an oxidizing agent.

The commercial material Evonik P25 (before Degussa P25), is by far the most used photocatalyst. It is constituted by a 3:1 ratio between the phases of TiO_2 anatase and rutile [1] and has the advantage of its low toxicity, high active area, stability and low cost. However, one of the main disadvantages of TiO_2 is the necessity of use light in the UV range for its activation. This makes energy consumption the

main expense of the process when using artificial light, or makes the process rather inefficient when using sunlight.

Nowadays, new methods are being used to extend the range of wavelengths, in which the TiO_2 is able to absorb light and thus make the ultraviolet and visible spectra usable. Some of the ways to achieve this are sensitization with dyes or coupling of semiconductors [2–5], synthesis of mesoporous TiO_2, the use of different morphologies of TiO_2 at the nanometric level, reduction of agglomeration in TiO_2 nanoparticles or treatments to modify its surface. Another process for achieving improvements in TiO_2 activity consists of doping the TiO_2 with metallic and non-metallic elements. To achieve this, various processes have been successfully used, such as mechanochemistry [6,7], centrifugation coating methods [8], or wet chemistry methods [9]. However, these methods of deposition have some limitations among which are included: Long processing times, low product homogeneity and the necessity to incorporate additional stages for the separation of impurities [10,11].

One technique for doping TiO_2 that avoids the aforementioned problems is atomic layer deposition (ALD) [12]. This technique uses two gas-phase reaction stages directly on the surface of the product (in this case the TiO_2 nanoparticles) to deposit the material layer by layer [13]. First, a first reactant or precursor is passed through the system that adheres to the TiO_2 surface until it reaches saturation. Subsequently, a purge of the excess precursor is carried out, thus, ensuring that only a thin film remains on the surface. Subsequently, the second reactant or precursor that reacts with the first one is dosed. Again, the system is re-purged, ensuring that only precursors remain attached to thin films on the surface. This cycle is repeated the desired number of times to control the thickness reached. Because each stage of precursor exposure saturates the surface with a monomolecular layer of that precursor, the reactions are self-limited, allowing controlling the deposition at the atomic level, giving rise to several very advantageous characteristics, such as excellent formability and uniformity, and thickness control of the film.

In this work, P25 particles were coated with SiO_2 using ALD carried out in a fluidized bed, in order to improve the photocatalysis efficiency. Once the modified P25 (P25-SiO_2) was obtained, its efficiency in bacterial inactivation and in the removal of methylene blue and methanol from the water was compared with that obtained for the use of commercial P25. Additionally, as the synthesis of the catalyst P25-SiO_2 supposes an increase in the total costs of the process, its immobilization in macroporous foams was carried out with the aim of enabling the reuse of the catalyst. The use of these foams has already been shown to lead to comparable efficiencies to those achieved with the use of suspended catalysts [5].

2. Results and Discussion

2.1. Catalyst Characterization

The incorporation of SiO_2 to the TiO_2 material was confirmed by elemental analysis of the materials using ICP-AES (Table 1). The results showed an average percentage of Si of 1.3 wt % (2.78 wt % of SiO_2).

On the other hand, with the aim of achieving a better understanding of the results, the optical properties of the catalysts were studied. Figure 1 shows the extinction coefficients obtained for P25 and P25-SiO_2 catalysts for different wavelengths in the 300 to 450 nm wavelength range. It can be observed that P25-SiO_2 shows an extinction coefficient 25% lower than P25 at 365 nm but maintaining the same trend in relation to wavelength. Although, the extinction coefficient is not a direct measurement of the photonic absorption, because it also includes the scattering of radiation, it can reasonably assumed that both materials would behave similarly from the scattering point of view, and therefore the absorption of the P25-SiO_2 is significantly lower. Consequently, considering that the absorption of radiation is the triggering step of the photocatalytic process, the incorporation of SiO_2 can potentially reduce the reaction rate.

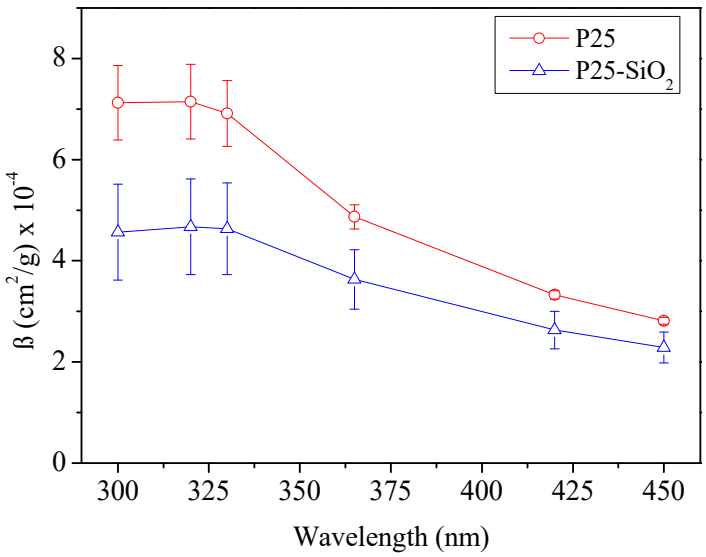

Figure 1. Napierian extinction coefficients for P25 and P25-SiO_2.

On the other hand, in order to check if the addition of SiO_2 produces a variation in the energy that is able to absorb the catalyst, the bandgap was obtained for the two catalysts. Figure 2a shows the diffuse reflectance spectra (DRS) of the three catalysts. Considering the proportionality between F(R) and the absorbance, it is possible to obtain the bandgap by extrapolation from the linear part of the reflectance spectrum represented as $(F(R) \times E)^{1/2}$ vs. E (Figure 2b), as described in bibliography [14].

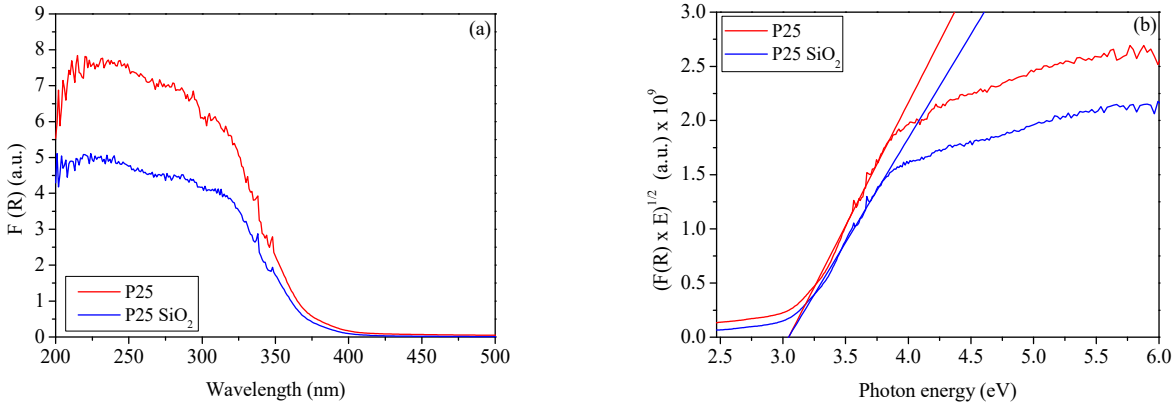

Figure 2. (**a**) DRS spectra; and (**b**) plot of transformed Kubelka–Munk function versus the energy of light for P25 and P25-SiO_2.

As shown in Table 1, bandgap values of 3.05 and 3.04 eV were obtained for P25 and P25-SiO_2, respectively. The values obtained are similar and agree with the bandgap values of the phases of TiO_2 anatase (3.2 eV) and rutile (3 eV), so it can be concluded that the addition of SiO_2 does not produce a significant change of the bandgap of the catalyst.

The textural properties of the catalysts were studied using the N_2 adsorption-desorption isotherms and are shown in Figure 3. How the obtained isotherms can be assimilated to an IUPAC type II isotherm can be observed, indicating the reduced porous character of the materials. The BET surface was calculated (Table 1) and values of 53.3 and 48.7 m^2/g were obtained for P25 and P25-SiO_2, respectively. The slightly smaller surface area of the modified catalyst can be easily explained considering that the addition of SiO_2 reduces the available surface.

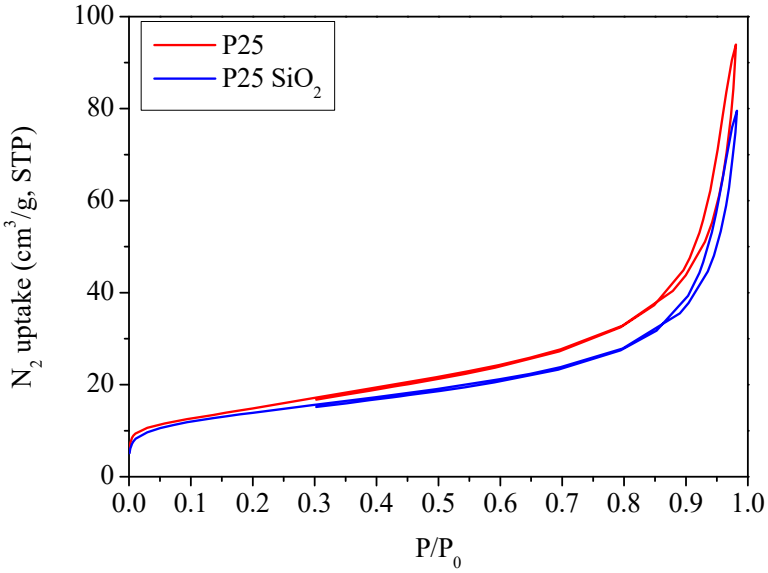

Figure 3. N_2 adsorption-desorption isotherms of P25 and P25-SiO_2.

The zeta potential value obtained for the P25 catalyst at natural pH was 18.1 mV, similar to values found in the literature [15]. However, in the case of the P25-SiO_2 catalyst, due to the negative potential of the silica [16], a final negative potential value of −3.7 mV was obtained. This fact is important, given the different zeta potential of both catalysts can concur in different ways of interacting with the pollutants to be degraded and therefore in different efficiencies in their removal. Moreover, the lower absolute value of the potential of the P25-SiO_2 facilitates the agglomeration of the catalyst particles, reducing the optical density of the suspensions and therefore the light absorption. Table 1 summarizes the main features of for both catalysts.

Table 1. Summary of the main features of P25 and P25-SiO_2.

Feature	TiO_2	SiO_2-TiO_2
SiO_2 (%)	0	2.78
β_{365nm} (cm^2/g)	48,700	36,300
Bandgap (eV)	3.05	3.04
S_{BET} (m^2/g)	53.3	48.7
Zeta Potential (mV)	18.1	−3.7

2.2. Photocatalytic Experiments

Photocatalytic experiments of methanol and methylene blue oxidation under solar irradiation with the catalysis in suspension were carried out in a reactor couple to a compound parabolic collector (CPC) (Figure 4). In the case of the methanol reaction test, no photolytic oxidation takes place [17]. Regarding methylene blue, it could present photolytic removal values of up to 10% [18,19], but this effect would be equivalent for both P25 and P25-SiO_2 materials, and therefore can be neglected for comparative purposes. On the other hand, methylene blue has been extensively studied under irradiation, and shows a certain generation of ROS [20,21] that would increase photocatalytic efficiency. However, again, this behavior is expected to be similar for the two catalysts used, so it can be ignored in this comparative study. Regarding *E. coli* inactivation, a comprehensive study of the analogies and differences between photocatalytic oxidation of chemicals and photocatalytic inactivation of microorganisms, using methylene blue and *E. coli* as target models can be found elsewhere, including the kinetic analysis of the process [22]. The results obtained for methylene blue were fitted to a first-order kinetic model with respect to the accumulated solar incident radiation, usual way of reporting the photocatalytic activity in solar processes [23]. On the other hand, results for methanol

oxidation were fitted using the formaldehyde production throughout the reaction following zero-order kinetics as detailed elsewhere [24]. The initial reaction rate for methylene blue was obtained by multiplying the calculated first-order kinetic constant by the initial concentration, whereas in the case of methanol oxidation the initial reaction rate was directly calculated from the fitting to a zero order kinetics of the formaldehyde concentration. The results show an improvement in methylene blue removal when using P25-SiO_2 with respect to the commercial P25. However, in the case of methanol oxidation, the opposite behaviour is observed: The methanol oxidation rate decreases (Figure 4).

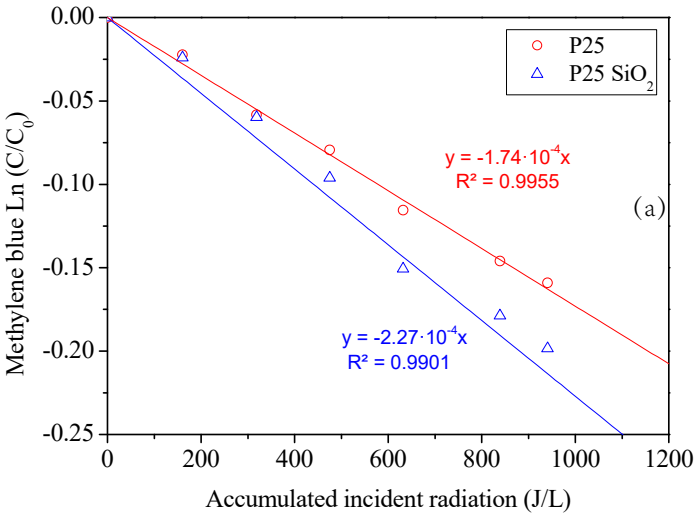

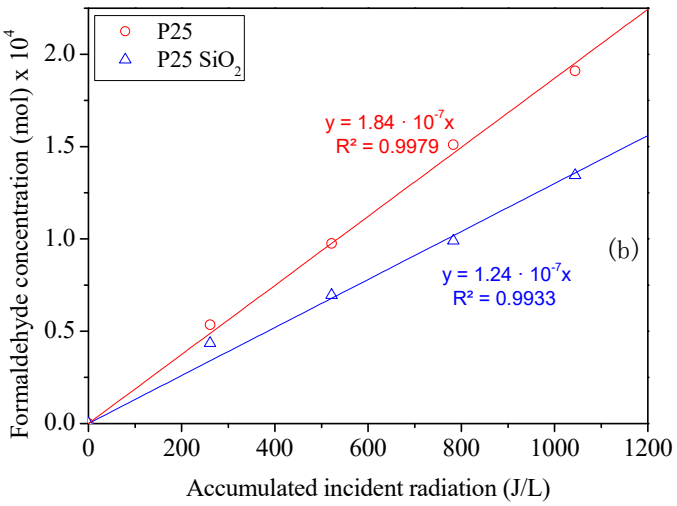

Figure 4. *Cont.*

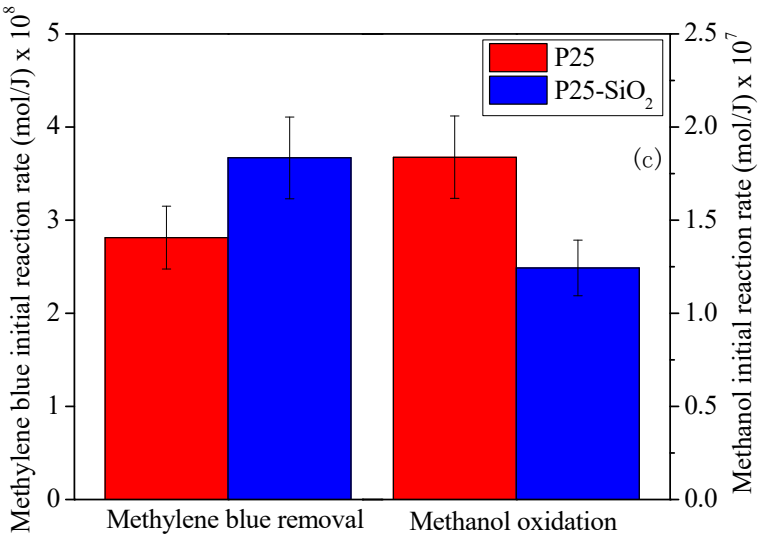

Figure 4. (**a**) First-order kinetic plot of methylene blue removal; (**b**) zero-order kinetic plot of formaldehyde formation; and (**c**) initial reaction rates for both reactions in a CPC reactor under solar irradiation. Error bars calculated from at least three replicate experiments.

Figure 1 shows how the addition of SiO_2 to the P25 catalyst did not modified the spectral response of the catalyst, and only an attenuation in the extinction coefficient was observed (Table 1).In addition, in Figure 2, the non-existence of clear differences in the bandgap values between both catalysts could be confirmed. Therefore, the difference in the results obtained for each catalyst, observed in Figure 4, seems to indicate the existence of different behavior of the catalysts when interacting with the two pollutants, and not the existence of differences in photonic absorption.

In order to find an explanation for the different behavior of the catalysts with each pollutant, similar photocatalytic reactions were carried out in an up-flow reactor, in which photocatalytic foams prepared with both catalysts could also be used. In this case, the light source was a lamp with 40 LEDs of 365 nm. Additionally, the application of the materials to bacterial inactivation processes was also studied to provide new insights. *E. coli* inactivation kinetics were calculated from the logarithmic inactivation profiles using the mechanistic model developed by Marugán et al. [25].

Figure 5a,b shows that results similar to those previously observed when using the CPC reactor under solar irradiation (Figure 4) were obtained, with an improvement in the removal of methylene blue with P25-SiO_2 catalyst, which was not observed in the methanol oxidation. These results confirm that the addition of SiO_2 to P25, do not lead to an amplification in the absorption spectra of the catalyst since the $k_{P25}/k_{P25\text{-}SiO2}$ ratio was similar for both solar and artificial 365 nm irradiation. On the other hand, in the case of bacterial inactivation, it could be observed (Figure 5c) that similar values were obtained for both catalyts.

The results of methanol oxidation tests show a reduction of approximately 25% of the efficiency when using P25-TiO_2 in comparison with the bare P25. This value is similar to the reduction of the extinction coefficient at 365 nm (Table 1), indicating that the decrease in the photocatalytic efficiency is due to the lower photon absorption rate upon incorporation of the SiO_2.

In contrast, in the case of methylene blue removal and E. coli inactivation it seems that the global efficiency is not exclusively limited by the photocatalytic process, suggesting that the adsorption and interaction with the catalyst could play a significant role.

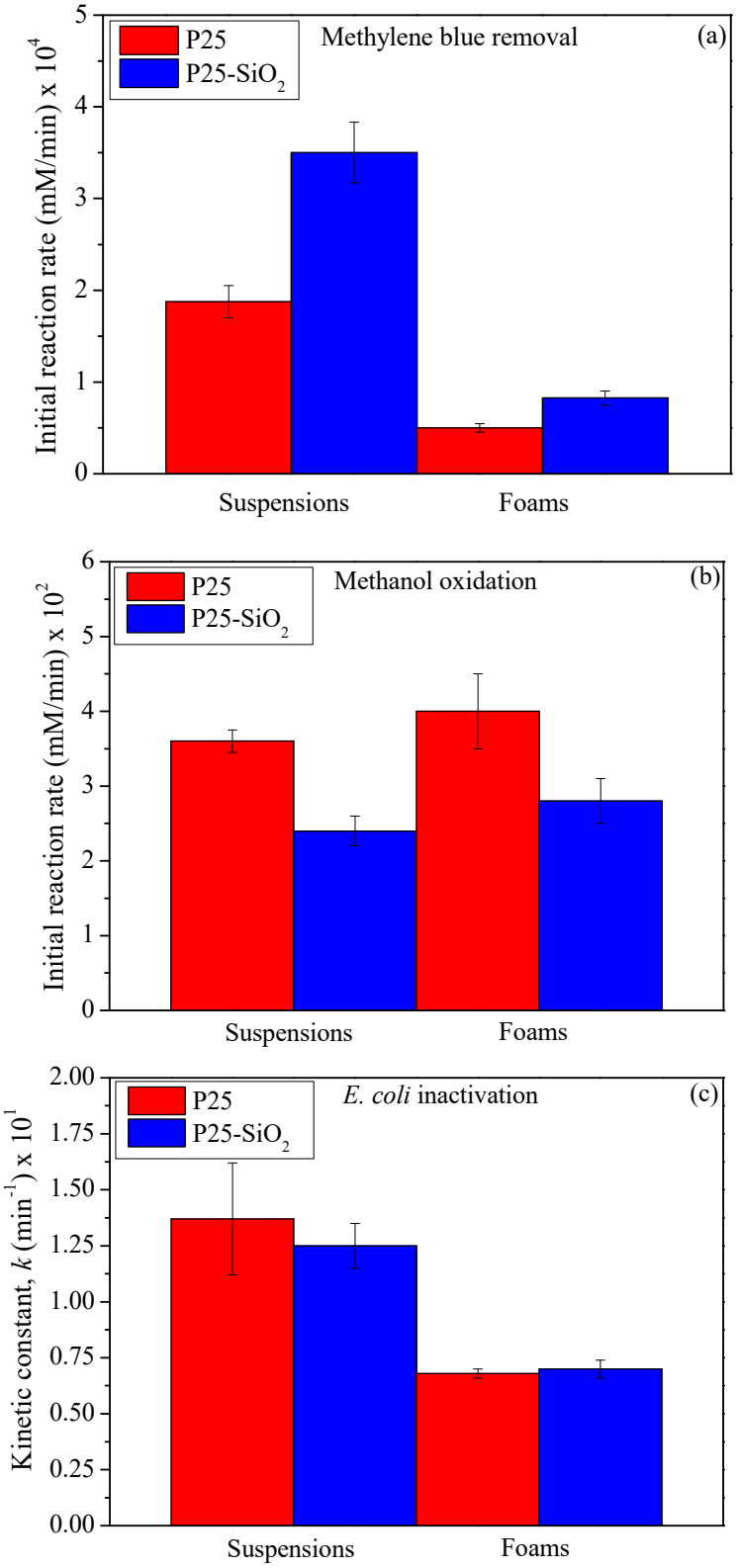

Figure 5. Initial reaction rate for; (**a**) methylene blue removal; and (**b**) methanol oxidation; and (**c**) kinetic constant bacterial inactivation (fitted from the logarithmic inactivation profiles according to Marugán et al. [23]) in an up-flow reactor under artificial 365 nm light. Error bars calculated from at least three replicate experiments.

Some studies have shown the efficiency of SiO_2 to carry out the removal of methylene blue from water by adsorption [26]. Furthermore, it has been demonstrated that the addition of SiO_2 to TiO_2 can improve the adsorption of contaminants [27]. On the other hand, the loss of photocatalytic efficiency that can result from the addition of SiO_2 to the TiO_2 surface, as observed in methanol oxidation, has also been revealed [28].

Taking into account the above, and trying to explain the obtained results, it was decided to carry out methylene blue adsorption experiments. Methylene blue solutions with different concentrations of both P25 and P25-SiO_2 were prepared and the evolution of methylene blue concentration was followed over time. The results shown in Figure 6 indicate that, due to the addition of SiO_2 to the catalyst structure, there is a considerable increase in the adsorption of the methylene blue, which increases the efficiency of its removal from water, arising from the combined effect of adsorption and photocatalytic decomposition. This behavior can be explained if we focus on the results obtained previously in relation to the zeta potential. It was observed that the zeta potential of P25 was positively charged, however, the addition of SiO_2 produced an alteration of the zeta potential that becomes negative (Table 1). Since methylene blue has a positive charge [29], it is easy to understand that it interacts much more with P25-SiO_2. Therefore, being the adsorption capacity of P25-SiO_2 much greater than in the case of P25. Thus, it is possible to explain the greater removal efficiency of methylene blue when using the P25-SiO_2 catalyst due to the synergistic combination of the adsorption and the photocatalytic reaction processes. This synergism accelerates the reaction due to the higher concentration of dye molecules on the catalysts surface, but also accelerates the adsorption due to the consumption of the adsorbed molecules by the reaction, releasing the active sites for the adsorption of new dye molecules. Similar results were obtained by Li et al. [30] in the removal of methylene blue using a P25-graphene composite. They observed that the removal of methylene blue was enhanced by the combination of adsorption and the photocatalytic process. The same conclusions were also reported by other research groups working with different TiO_2 modifications [31,32]. In any case, considering that the reaction time of the photocatalytic experiments is 30 min, and that time is not sufficient to reach the adsorption equilibrium (Figure 6), it cannot be discarded that long-term experiment could present a saturation effect.

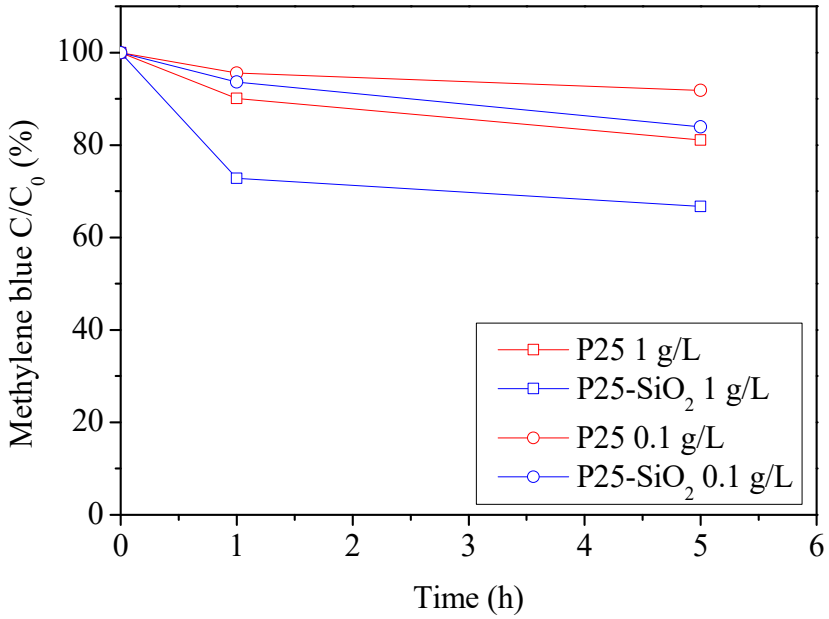

Figure 6. Adsorption of methylene blue along time for different concentrations of P25 and P25-SiO_2.

A similar behaviour may explain the higher efficiency obtained in the *E. coli* inactivation, compared to that expected if only the photocatalytic efficiency is taken into account. Several studies have focused on the adhesion of the bacteria *E. coli* on SiO_2 materials [33,34], showing that the addition of SiO_2 to P25

makes the adhesion of *E. coli* bacteria on the surface of the catalyst became more thermodynamically favorable. Additionally, a higher antibacterial activity was observed for adhered E. coli cells than the suspended cells in aqueous phase, which was explained by the short half-life of reactive oxygen species and slow diffusion in aqueous phase [35].

In relation to the use of photocatalytic foams, Figure 5 shows an inevitable reduction in the removal efficiency of pollutants in comparison with the suspended catalysts, due to a reduction in the surface area available for the reaction. However, the results show very similar removal efficiencies for both catalysts and the loss in activity can be counteracted by the advantages of the use of the immobilized photocatalyst. The deposition of commercial P25 and othersTiO_2 materials on the foam template and its stability through subsequent reaction cycles has been demonstrated in previous work [36].

3. Materials and Methods

3.1. Atomic Layer Deposition

The modification of P25 particles was carried out by adding SiO_2 by ALD. ALD consists of two gas-phase reaction stages directly on the surface of the product to deposit the material layer by layer [37]. For this, a fluidized bed, consisting of a glass column of 25 mm in diameter and 500 mm in length was used. A metal connection was placed in the lower part of the column and in the upper part where the input and output lines were connected. This connection included a distributor plate SIKA-R 20 AX to avoid the exit of the particles to the outside of the reactor and to ensure homogeneous gas distribution at the column entry. The column was placed on a vibrating table Straw PTL 40 / 40-24 (frequency: 35 Hz) to help fluidize the particles. The metal precursor used was $SiCl_4$; it was kept in a stainless steel bubbler (Strem Chemicals, Inc., Newburyport, MA, USA) under an inert gas atmosphere. Pneumatic valves were used to control the flow of gas in and out of the column. The metal precursor and the purge inlet flow contained nitrogen (N_2, grade 5.0), while the oxidizer (precursor 2) inlet flow contained wet N_2. The glass column was heated to 100 °C with an infrared lamp.

To carry out the SiO_2 deposition, 5 g of P25 was introduced into the interior of the column and 8 reaction cycles were carried out. Each reaction cycle consisted of a 30 s dosage of the metal precursor, followed by 5 min of purging. Later, a 3 min dose of oxidant precursor followed by a purge with nitrogen of 8 min. Both the reaction temperatures, the number of cycles and the dosing time of each precursor were previously optimized [38].

3.2. Photocatalytic Experiments

Three different contaminants were tested throughout this study with the aim of having a clear vision of the effects produced by incorporating SiO_2 into commercial P25. On the one hand, chemical oxidation experiments were carried out using both, methylene blue and methanol. The initial concentration of methylene blue and methanol was 0.05 mM, and 100 mM, respectively and the solutions were prepared in deionized water. Photocatalytic degradation of methylene blue was monitored by direct measurement of the absorption at 664 nm in a spectrophotometer while methanol oxidation was followed through the colorimetric determination of the formaldehyde produced throughout the reaction, which is a quantitative oxidation product when methanol is in excess [24]. In addition, bacterial inactivation experiments were carried out. Synthetic wastewater was prepared by adding *E. coli* K12 (CECT 4624, corresponding to ATCC 23631) with an initial concentration of 10^6 CFU/mL. Fresh liquid cultures of *E. coli* were prepared by inoculation in Luria-Bertani (LB) nutrient medium (Miller's LB Broth, Scharlab) and incubation at 37 °C for 24 h under constant stirring on a rotary shaker. The concentration of viable bacteria was quantified throughout the reaction according to the standard serial dilution procedure. Each decimal dilution was spotted 8 times on LB agar plates and incubated at 37 °C before counting after 24 h.

Both the photocatalytic activity of P25 and P25-SiO_2 was tested using two configurations: (i) in suspension and (ii) supported onto three-dimensional (3D) foams (in order to avoid the loss of the

photocatalyst). When using the suspensions in all cases, the catalyst concentration was 0.10 g/L and the suspensions were sonicated for 30 min before the reaction.

3.3. Photocatalytic Reactors

A compound parabolic collector (CPC) reactor that operates under sunlight was used to check whether the addition of SiO_2 involved an improvement in the P25 absorption of the solar spectrum. The CPC has two differentiated circuits, in which experiments were carried out simultaneously with P25 and P25-SiO_2 to ensure comparison under exactly the same sunlight conditions. Each circuit has a borosilicate 3.3 Duran®glass tube placed in the focal line of the CPC collector with a length of 380 mm and an inner diameter of 26 mm [39]. The reactor was operated in a closed recirculating circuit driven with a reservoir tank, being the total working volume of 1 L. The experiments were carried in June 2019 at Universidad Rey Juan Carlos facilities in Mostoles, Spain (40.33° N, 3.88° W). The solar irradiance was monitored during the reaction time with a spectrophotometer (Blue Wave, StellarNetInc., Tampa, FL, USA).

An up-flow annular reactor (15 cm long, 3 cm inner diameter and 5 cm outer diameter) was also used. The reactor operated in a closed recirculating circuit driven with a reservoir tank, being the total working volume of 1 L. As illumination source, a 40 LED system (LedEngin Model LZ1-00UV00) with maximum emission peak centered in 365 nm was placed in the axis of the reactor. This reactor allows the operation not only with the catalyst in suspension but also with the photocatalytic foams, as reported elsewhere [36].

3.4. Foams Coating

Macroporous ZnO foams supplied by Insertec SA (2.5 cm height, 3 cm inner diameter, 5 cm outer diameter and a porosity of 10 ppi were coated with P25 and modified P25 (P25-SiO_2) according to the procedure described in a previous work [5]. First, catalyst solutions were prepared in distilled water at a concentration of 10 g/L, and then the foam template was dipped in the solutions and removed after a few seconds. The excess of catalyst was removed by the use of air. Then, the foams were dried for two hours at 100 °C and subsequently calcined for two hours at 500 °C. The amount of catalyst deposited in each foam was measured by weighing difference and the procedure was repeated until reach a total weight in each foam close to 1 g as was previously established as optimum in a previous work where it was also concluded that the foam templates does not show any photocatalytic activity [5]. The photocatalytic experiments for each catalyst were carried out using six foams being the total working height 15 cm.

3.5. Characterization Techniques

The amount of Si deposited in the TiO_2 was measured by inductively coupled plasma atomic emission spectroscopy (ICP-AES) using a Perkin Elmer Optima 4300DV instrument (nebulizer: PE / injector: Al_2O_3). Approximately 30 mg of sample was dissolved in 4.5 mL 30% HCl + 1.5 mL 65% HNO_3 + 0.2 mL 40% HF using a microwave during 60 min. After dissolution the samples were diluted to 50 mL with deionized water and analyzed by ICP-AES.

The specific extinction coefficients (β*) of the catalysts were obtained using the direct measurement of the transmittance of suspensions with increasing concentration of the material in a UV/vis spectrophotometer (UV-Vis-NIR Varian Cary 500).

Nitrogen adsorption-desorption isotherms were measured using an AutoSorb equipment (Quantachrome Instruments). Degassing of the materials prior to the analysis was carried out by heating at 373 K and applying vacuum until 1×10^{-3} kPa. The surface area was calculated by using the Brunauer–Emmett–Teller (BET) model using the adsorption branch. Zeta potential values were measured using a NanoPlus DLS Zeta Potential equipment to determine the electrostatic interactions among catalysts and methylene blue. Measurements were taken with catalysts suspensions in the same experimental conditions than the reaction tests.

4. Conclusions

Atomic layer deposition was used for adding SiO_2 to the surface of P25. Due to the incorporation of the silica layer, a loss of photocatalytic efficiency took place as observed in the results obtained for the oxidation of methanol. However, the incorporation of SiO_2 also improves the adhesion of bacteria to the surface of the material, partially counteracting the decrease in the photocatalytic activity and leading to a comparable global inactivation rate. Moreover, the SiO_2 layer improves significantly the adsorption of methylene blue, increasing the global removal rate with respect to the bare P25 material as a results of the combination of adsorption and photocatalytic oxidation.

On the other hand, both catalysts show only a small loss of photocatalytic efficiency when immobilized in a macroporous foam as catalytic support. This 3D catalytic system provides the next step towards implementation of the photocatalytic process in a reusable structured reactor configuration without the necessity of a recovery stage of the dispersed catalyst particles.

Author Contributions: Methodology, M.M.-S. and D.B.; data curation, J.M. and J.R.v.O.; writing—original draft preparation, M.M.-S.; writing—review and editing, M.M.-S., D.B., J.R.v.O. and J.M.; supervision, J.M. and J.R.v.O.; funding acquisition, J.M. and J.R.v.O. All authors have read and agreed to the published version of the manuscript.

Funding: This research is supported by the TU Delft | Global Initiative, a program of the Delft University of Technology to boost Science and Technology for Global Development. The authors gratefully acknowledge the financial support of the Spanish State Research Agency (AEI) and the Spanish Ministry of Science and Universities through the CALYPSOL-ATECWATER project (RTI2018-097997-B-C33) and Comunidad de Madrid through the program REMTAVARES (P2018/EMT-4341). Dr. Martín-Sómer also acknowledges MECD for its FPU grant (FPU014/04389) and Universidad Rey Juan Carlos for funding his research stay at the TU Delft.

Conflicts of Interest: The authors declare no conflict of interest.

References

1. Ohno, T.; Sarukawa, K.; Tokieda, K.; Matsumura, M. Morphology of a TiO_2 photocatalyst (Degussa, P25) consisting of anatase and rutile crystalline phases. *J. Catal.* **2001**, *203*, 82–86. [CrossRef]
2. Daghrir, R.; Drogui, P.; Robert, D. Modified TiO_2 for environmental photocatalytic applications: A review. *Ind. Eng. Chem. Res.* **2013**, *52*, 3581–3599. [CrossRef]
3. Marschall, R.; Wang, L. Non-metal doping of transition metal oxides for visible-light photocatalysis. *Catal. Today* **2014**, *225*, 111–135. [CrossRef]
4. Pelaez, M.; Nolan, N.T.; Pillai, S.C.; Seery, M.K.; Falaras, P.; Kontos, A.G.; Dunlop, P.S.M.; Hamilton, J.W.J.; Byrne, J.A.; O'Shea, K.; et al. A review on the visible light active titanium dioxide photocatalysts for environmental applications. *Appl. Catal. B Environ.* **2012**, *125*, 331–349. [CrossRef]
5. Rehman, S.; Ullah, R.; Butt, A.M.; Gohar, N.D. Strategies of making TiO_2 and ZnO visible light active. *J. Hazard. Mater.* **2009**, *170*, 560–569. [CrossRef]
6. Osman, Y.; Jamal, R.; Rahman, A.; Xu, F.; Ali, A.; Abdiryim, T. Comparative study on poly(3,4-propylenedioxythiophene)/TiO_2 nanocomposites synthesized by mechanochemical and chemical solution methods. *Synth. Met.* **2013**, *179*, 54–59. [CrossRef]
7. Cheng, L.; Qiu, S.; Chen, J.; Shao, J.; Cao, S. A practical pathway for the preparation of Fe_2O_3 decorated TiO_2 photocatalyst with enhanced visible-light photoactivity. *Mater. Chem. Phys.* **2017**, *190*, 53–61. [CrossRef]
8. Li, X.; Lin, H.; Chen, X.; Niu, H.; Liu, J.; Zhang, T.; Qu, F. Dendritic α-Fe_2O_3//TiO_2 nanocomposites with improved visible light photocatalytic activity. *Phys. Chem. Chem. Phys.* **2016**, *18*, 9176–9185. [CrossRef]
9. Cheng, G.; Xu, F.; Xiong, J.; Wei, Y.; Stadler, F.J.; Chen, R. A novel protocol to design TiO_2-Fe_2O_3 hybrids with effective charge separation efficiency for improved photocatalysis. *Adv. Powder Technol.* **2017**, *28*, 665–670. [CrossRef]
10. Michalchuk, A.A.L.; Tumanov, I.A.; Konar, S.; Kimber, S.A.J.; Pulham, C.R.; Boldyreva, E.V. Challenges of mechanochemistry: Is in situ real-time quantitative phase analysis always reliable? A case study of organic salt formation. *Adv. Sci.* **2017**, *4*, 1700132. [CrossRef]
11. Ritala, M.; Leskelä, M. Atomic layer deposition. *Handb. Thin Film.* **2002**, *409*, 103–159.
12. Grillo, F.; Kreutzer, M.T.; van Ommen, J.R. Modeling the precursor utilization in atomic layer deposition on nanostructured materials in fluidized bed reactors. *Chem. Eng. J.* **2015**, *268*, 384–398. [CrossRef]

13. van Ommen, J.R.; Goulas, A. Atomic layer deposition on particulate materials. *Mater. Today Chem.* **2019**, *14*, 100183. [CrossRef]
14. Valencia, S.; Marín, J.M.; Restrepo, G. Study of the bandgap of synthesized titanium dioxide nanoparticules using the sol-gel method and a hydrothermal treatment. *Open Mater. Sci. J.* **2010**, *4*, 9–14. [CrossRef]
15. Kalpaklı, Y.K.; Akgun, M.; Köneçoğlu, G.; Toygun, Ş.; Kalpaklı, Y.; Akgün, M. Photocatalytic degradation of textile dye CI Basic Yellow 28 wastewater by Degussa P25 based TiO_2. *Adv. Environ. Res.* **2015**, *4*, 25–38.
16. Martín, A.; Morales, V.; Ortiz-Bustos, J.; Pérez-Garnes, M.; Bautista, L.F.; García-Muñoz, R.A.; Sanz, R. Modelling the adsorption and controlled release of drugs from the pure and amino surface-functionalized mesoporous silica hosts. *Microporous Mesoporous Mater.* **2018**, *262*, 23–34. [CrossRef]
17. Martín-Sómer, M.; Vega, B.; Pablos, C.; van Grieken, R.; Marugán, J. Wavelength dependence of the efficiency of photocatalytic processes for water treatment. *Appl. Catal. B Environ.* **2018**, *221*, 258–265. [CrossRef]
18. Houas, A.; Lachheb, H.; Ksibi, M.; Elaloui, E.; Guillard, C.; Herrmann, J.M. Photocatalytic degradation pathway of methylene blue in water. *Appl. Catal. B Environ.* **2001**, *31*, 145–157. [CrossRef]
19. Soltani, T.; Entezari, M.H. Photolysis and photocatalysis of methylene blue by ferrite bismuth nanoparticles under sunlight irradiation. *J. Mol. Catal. A Chem.* **2013**, *377*, 197–203. [CrossRef]
20. McCaughan, B.; Rouanet, C.; Fowley, C.; Nomikou, N.; McHale, A.P.; McCarron, P.A.; Callan, J.F. Enhanced ROS production and cell death through combined photo- and sono-activation of conventional photosensitising drugs. *Bioorg. Med. Chem. Lett.* **2011**, *21*, 5750–5752. [CrossRef]
21. May, J.M.; Qu, Z.C.; Whitesell, R.R. Generation of oxidant stress in cultured endothelial cells by methylene blue: Protective effects of glucose and ascorbic acid. *Biochem. Pharmacol.* **2003**, *66*, 777–784. [CrossRef]
22. Marugán, J.; van Grieken, R.; Pablos, C.; Sordo, C. Analogies and differences between photocatalytic oxidation of chemicals and photocatalytic inactivation of microorganisms. *Water Res.* **2010**, *44*, 789–796. [CrossRef] [PubMed]
23. Jouali, A.; Salhi, A.; Aguedach, A.; Aarfane, A.; Ghazzaf, H.; Lhadi, E.K.; el krati, M.; Tahiri, S. Photo-catalytic degradation of methylene blue and reactive blue 21 dyes in dynamic mode using TiO_2 particles immobilized on cellulosic fibers. *J. Photochem. Photobiol. A Chem.* **2019**, *383*, 112013. [CrossRef]
24. Pablos, C.; Marugán, J.; van Grieken, R.; Adán, C.; Riquelme, A.; Palma, J. Correlation between photoelectrochemical behaviour and photoelectrocatalytic activity and scaling-up of P25-TiO_2 electrodes. *Electrochim. Acta* **2014**, *130*, 261–270. [CrossRef]
25. Marugán, J.; van Grieken, R.; Sordo, C.; Cruz, C. Kinetics of the photocatalytic disinfection of *Escherichia coli* suspensions. *Appl. Catal. B Environ.* **2008**, *82*, 27–36. [CrossRef]
26. Xiong, J.; Li, G.; Hu, C. Treatment of methylene blue by mesoporous Fe/SiO_2 prepared from rice husk pyrolytic residues. *Catal. Today.* **2019**. [CrossRef]
27. Nishikawa, H.; Takahara, Y. Adsorption and photocatalytic decomposition of odor compounds containing sulfur using TiO_2/SiO_2 bead. *J. Mol. Catal. A Chem.* **2001**, *172*, 247–251. [CrossRef]
28. Yaparatne, S.; Tripp, C.P.A. Amirbahman, Photodegradation of taste and odor compounds in water in the presence of immobilized TiO_2-SiO_2 photocatalysts. *J. Hazard. Mater.* **2018**, *346*, 208–217. [CrossRef]
29. Uddin, M.T.; Islam, M.A.; Mahmud, S.; Rukanuzzaman, M. Adsorptive removal of methylene blue by tea waste. *J. Hazard. Mater.* **2009**, *164*, 53–60. [CrossRef]
30. Li, J.; Zhou, S.L.; Hong, G.B.; Chang, C.T. Hydrothermal preparation of P25-graphene composite with enhanced adsorption and photocatalytic degradation of dyes. *Chem. Eng. J.* **2013**, *219*, 486–491. [CrossRef]
31. Nguyen, C.H.; Juang, R.S. Efficient removal of methylene blue dye by a hybrid adsorption–photocatalysis process using reduced graphene oxide/titanate nanotube composites for water reuse. *J. Ind. Eng. Chem.* **2019**, *76*, 296–309. [CrossRef]
32. Ngoh, Y.S.; Nawi, M.A. Fabrication and properties of an immobilized P25 TiO_2-montmorillonite bilayer system for the synergistic photocatalytic-adsorption removal of methylene blue. *Mater. Res. Bull.* **2016**, *76*, 8–21. [CrossRef]
33. Jucker, B.A.; Harms, H.; Hug, S.J.; Zehnder, A.J.B. Adsorption of bacterial surface polysaccharides on mineral oxides is mediated by hydrogen bonds. *Colloids Surf. B Biointerfaces* **1997**, *9*, 331–343. [CrossRef]
34. Huang, T.T.; Sturgis, J.; Gomez, R.; Geng, T.; Bashir, R.; Bhunia, A.K.; Robinson, J.P.; Ladisch, M.R. Composite surface for blocking bacterial adsorption on protein biochips. *Biotechnol. Bioeng.* **2003**, *81*, 618–624. [CrossRef] [PubMed]

35. Erdural, B.; Bolukbasi, U.; Karakas, G. Photocatalytic antibacterial activity of TiO_2-SiO_2 thin films: The effect of composition on cell adhesion and antibacterial activity. *J. Photochem. Photobiol. A Chem.* **2014**, *283*, 29–37. [CrossRef]
36. Martín-Sómer, M.; Pablos, C.; de Diego, A.; van Grieken, R.; Encinas, Á.; Monsalvo, V.M.; Marugán, J. Novel macroporous 3D photocatalytic foams for simultaneous wastewater disinfection and removal of contaminants of emerging concern. *Chem. Eng. J.* **2019**, *366*, 449–459. [CrossRef]
37. Grillo, F.; Moulijn, J.A.; Kreutzer, M.T.; van Ommen, J.R. Nanoparticle sintering in atomic layer deposition of supported catalysts: Kinetic modeling of the size distribution. *Catal. Today* **2018**, *316*, 51–61. [CrossRef]
38. Guo, J.; van Bui, H.; Valdesueiro, D.; Yuan, S.; Liang, B.; van Ommen, J. Suppressing the photocatalytic activity of TiO_2 nanoparticles by extremely thin Al_2O_3 films grown by gas-phase deposition at ambient conditions. *Nanomaterials* **2018**, *8*, 61. [CrossRef]
39. Philippe, K.K.; Timmers, R.; van Grieken, R.; Marugan, J. Photocatalytic disinfection and removal of emerging pollutants from effluents of biological wastewater treatments, using a newly developed large-scale solar simulator. *Ind. Eng. Chem. Res.* **2016**, *55*, 2952–2958. [CrossRef]